

3.

EXPERIMENT3.1 Introduction

Experimental measurements of the vibrational and chemical relaxation rates of N_2 are presented in this chapter. In section 3.2, free-piston shock tube measurements of N_2 dissociation rates, using time-resolved optical interferometry, are described (see also Kewley and Hornung 1974a). The vibrational de-excitation and excitation rates of N_2 are investigated in the small free-piston shock tunnel T2, using optical interferograms of flow over a wedge in the hypersonic nozzle expansion; this work is given in section 3.3. The dissociation rates of nitrogen are measured from optical interferograms of flow over a wedge, in the large free-piston shock tunnel T3 (see also Kewley and Hornung 1974b). These results and an analysis of Crane's (1975) measurements of nitrogen atom mass fraction and helium contamination in T3 are presented in section 3.4.

The aim of the experimental work is to carry out the projects suggested in the Historical Review (section 1.2) and listed in section 1.3. In doing so, the experiments also provide a test of the reliable running conditions for the free-piston technique.

3.2 DDT Shock Tube Experiments

The chief motivation for measuring the dissociation rate of nitrogen at high temperatures has been its importance in flows occurring during re-entry into the Earth's atmosphere. A number of authors (Byron 1966, Cary 1965 and 1966, Appleton, Steinberg and Liquornik 1968 and Hanson and Baganoff 1972) have made measurements of the rates for the reactions



covering temperatures ranging up to 15000K, and the disparity between different authors' results is well outside their estimated uncertainties. Allen, Keck and Camm (1962) give a value of k_d^{N} at 6400K only but, according to Carlson and Rieper (1972), it is likely to be 6 times too fast.

In an evaluation of previous experimental results it must be remembered that different authors inferred the dissociation rates from measurements of different quantities. Moreover, the results were taken under a variety of experimental conditions. In particular, dilution of N_2 with an inert gas, usually argon, has been widely employed to various degrees in order to achieve higher temperatures in shock tubes. To illustrate the range over which experimental results have been obtained, Figure 3.1 shows a plot of nitrogen concentration in the gas studied, against temperature achieved. It can be seen that the major part of the high temperature results (above say 10000K) has been obtained with an inert gas dilution of at least 80%, the exception being the pressure measurements of Hanson and Baganoff (1972) at zero dilution. No results using incident shock interferometry are available above 10000K. There is thus a need to try this technique at higher temperatures, preferably at zero dilution. It is particularly important to extend such an investigation over a large range of temperature, because the various authors disagree most about the temperature dependence of the reaction rates. Hanson and Baganoff (1972), whose experiments span

the widest temperature range, observe an unusually strong pre-exponential temperature dependence of the rates for both reactions 3.2-1 and 2 by their reflected shock pressure measurement technique. Similar dependences have been found for dissociation of undiluted O_2 (see Stupochenko et al. 1967 p154) and CO (Hanson 1973).

The aim of this section (3.2) is to obtain nitrogen dissociation rate measurements by incident shock time-resolved optical interferometry in the free-piston shock tube DDT, described by Sandeman and Allen (1971), operating in the single diaphragm mode. The advantages offered by the free-piston technique are that shock speeds of $4-10 \text{ km sec}^{-1}$ can be achieved in nitrogen at the comparatively high initial pressures of 42-2 torr. (This is to be compared with $4-7 \text{ km sec}^{-1}$ into 5-0.5 torr for the combustion driven shock tubes of Hanson and Baganoff (1972).) Thus, one obtains a comparatively high fringe shift which enables rates to be measured accurately. The method also provides a very large temperature range in which the unusual temperature dependence observed by Hanson and Baganoff (1972) can be tested. However the induction time for nitrogen observed by Hornung (1972a) is predicted to be too small to be resolved.

3.2.1 Relaxation Rate Model and Numerical Calculations

The form of the expression for the dissociation rate is taken to be the same as Equation 2.6-31

$$D\alpha/Dt = \rho \{ k_d^{N_2} (1-\alpha) + 2k_d^{N\alpha} \} ((1-\alpha) - 4\rho\alpha^2/W_{N_2} K(T)) / W_{N_2} .$$

(3.2-3)

The rate coefficients are

$$k_d^{N_2} = C_1 T^{-n_1} \exp(-\theta_d/T), \quad (3.2-4)$$

$$k_d^N = C_2 T^{-n_2} \exp(-\theta_d/T), \quad (3.2-5)$$

where the C's and n's are to be determined from comparisons with experiment; θ_d is taken to be 113200K. It should be noted that Equation 3.2-3 assumes a linear rate law (see section 2.4.1).

In the present range of interest, two other rate processes are important in the post-shock relaxation region. The first, occurring mainly very close to the shock, is vibrational relaxation for which the Landau-Teller model and rates of Appleton (1967) are used. The second is ionization, which might be neglected energetically, but must be taken into account to determine the contribution to the fringe shift by the presence of electrons. The electron-producing reactions considered are the ionization of both N_2 and N by N_2 , N and electrons as well as dissociative recombination. The rates for all these 7 reactions are taken to be those recommended in Dunn and Lordi (1970).

The numerical computer program of Garr and Marrone (1963) and Garr et al. (1966) (NSHOCK) briefly described in section 2.6.2 is used. This program was also used in Chackerian (1971) and Carlson and Rieper (1972) and permits simultaneous vibrational and chemical relaxation. Here the option of coupling is not used, to make comparisons with past work valid. A calculation for a particular set of initial conditions and for an assumed set of values of C and n results in a distribution of the gas properties with distance, s , downstream of the shock (shock-fixed coordinates). This distribution may then be used to calculate the expected fringe

shift, on an interferogram, between the free-stream and a point behind the shock from

$$f(s) = A \ell (\rho - \rho_\infty) (1 + 0.28\alpha) / \lambda \quad (3.2-6)$$

where ℓ is the geometrical path length of the light beam, λ is the wavelength of the light used and ρ_∞ is the density upstream of the shock. A is a constant equal to $0.240 \text{ cm}^3 \text{ g}^{-1}$. This value and the coefficient of α in Equation 3.2-6 are derived from the refractivities of N_2 and N as given in Alpher and White (1959) and Wettlaufer (1972). In cases where the contribution to the fringe shift from electrons is significant, the following additive correction to f is made:

$$f_e = -B \ell \lambda n_e \quad (3.2-7)$$

where n_e is the electron number density and B is a constant equal to $4.48 \times 10^{-14} \text{ cm}$.

To compare the computed $f(s)$ with a time-resolved interferogram, the distance, x , along the time axis of the interferogram (corresponding to laboratory time t_ℓ) has to be related to s . It can be shown (Stupochenko et al. 1967 p.109) that laboratory time t_ℓ is related to particle time t_p by

$$t_\ell = \int_0^{t_p} (\rho_\infty / \rho) dt_p \quad (3.2-8)$$

In shock-fixed coordinates the continuity equation is

$$\rho_\infty U_\infty = \rho u \quad (3.2-9)$$

where U_∞ is the free-stream velocity and u is the shock-fixed velocity, which is equal to ds/dt_p . Thus s is given

by

$$s = \int_0^{t_p} u dt_p = U_\infty t_\ell = U_\infty x / v \quad (3.2-10)$$

where v is the sweep speed of the time-resolved interferogram.

3.2.2 Experiment

The shock tube used consists of a free-piston helium driver and a 4 cm diameter shock tube of 4.3m length. The stainless steel tube is operated in the single diaphragm mode instead of the double diaphragm mode of Sandeman and Allen (1971). A detailed description of the free-piston technique may be found in Stalker (1966).

The flow after the primary shock is studied by placing a Carl Zeiss Mach-Zehnder interferometer across the shock tube such that the end of the tube is in the field of view. The shock tube windows have a matching pair in the compensating chamber of the interferometer. A slit of 0.17mm width is imaged just past the end of the shock tube, at right angles to the flow, and the resulting interferogram is time-resolved by an STL image converter camera in the streak mode, with a sweep time range of 2 to 10 μ sec and a field of view of 25 \times 50mm. The ultimate time resolution limit at a sweep speed of 10 μ sec is 0.03 μ sec. The light source for this system is an exploding 1cm piece of copper wire ($9\Omega/m$) powered by a 400 μ F oil-filled capacitor charged to 5kV. It produces a flash of 50 to 100 μ sec duration and, like the image converter camera, is triggered with a suitable delay by the last shock timing station. A 5100 $\overset{\circ}{\text{A}}$ interference filter of 40 $\overset{\circ}{\text{A}}$ bandwidth is introduced into the system on the downbeam side of the interferometer. The interferograms are taken on Ilford HP4 film and developed at least six minutes in DK60A.

Shock timing using the photodiodes of Sandeman and Allen (1971) and Meier (1973) was found to be inadequate for

the lower shock tube initial pressures used here for the rate measurements (the pressure is a factor of 4 lower). Initially pressure transducers were tried but for most of the experiments presented ionization probes are used. The probe consists of two pins of nickel wire, set 2mm apart, in a nylon plug (see Stalker 1974). A capacitor is connected between the pins and is charged to a potential of between 30 and 50 volts. When a shock wave passes the probe the gas causes a sudden drop in the voltage between the pins. The probes are recessed in small cavities in the shock tube wall, which previously held the fibre-optic light-guides of the photodiode probes. The shock speed is measured to an accuracy of $\pm 0.5\%$ by timing the shock passage between three timing stations over the last 2m of the tube.

The shock tube is evacuated to a pressure of less than 10^{-4} torr before each shot and isolated for a few minutes for leak testing before filling it with the test gas. The lowest filling pressure is 2 torr. The initial gas temperature is in the range 296-303K.

3.2.3 Results

Because the geometrical optical path varies across the circular shock tube, a complete density field must be determined by a deconvolution of the axial symmetry by an Abel inversion. This was done for a number of gases including nitrogen by Meier (1973) who used the same experimental setup. His results show that the density calculated from the centre-line fringe shift, with the shock tube diameter as the geometrical path, agrees with the core value to good accuracy. At the small distances of interest here ($s < 3\text{mm}$) they agree within $\pm 2\%$.

The equilibrium density ratio ρ_e/ρ_∞ as determined from the asymptotic centre-line fringe shift and Equation 3.2-6 is plotted against shock speed in Figure 3.2 and compared with the calculated value. The agreement is seen to be within the estimated error bars, thus confirming the measured shock speeds and the equilibrium thermodynamics model (Garr and Marrone 1963 and section 2.6.1). Curves I and II correspond to driver conditions with 2700 lbs/in² and 10500 lbs/in² diaphragm burst pressures, respectively. The density for curve II is thus about four times as high as for curve I at the same shock speed. Unfortunately, this makes the relaxation time for II so short as to be impossible to resolve with the present setup.

The measured approach to equilibrium for the three interferograms shown in Figure 3.3 is presented in Figure 3.4. (Twenty-two other interferograms are also used in the analysis.) The calculated fringe shift according to the rates of Appleton et al. (1968) and Hanson and Baganoff (1972) is also shown. In all cases (including the ones not shown) the experimental points fall mainly between these two curves. However, because the fringe shift is lower and these curves converge at high temperature, the experiment is barely able to resolve between them at high shock speeds.

In order to determine the values of the C's and n's which fit the present results best, the procedure described in Hanson and Baganoff (1972) is adopted. This curve-fitting procedure is open to criticism on the grounds that it is too subjective and not demonstrably unique. Therefore methods such as those given by Hurle, Jones and Rosenfeld (1969) should be considered, in which either the curve-fitting

is reduced to a numerical non-linear estimation problem or the data is expressed as an analytic function of time.

However, for the 4 unknowns here it is not considered worthwhile (Hurle et al. 1969 had 6 unknowns to find). The first approximation to each of the rate coefficients is obtained from data in the regions where it is known to dominate.

(If this were not possible then a more sophisticated procedure would be needed.) Subsequent iterations are obtained by applying both rate coefficients to data at intermediate cases. This leads to

$$k_d^{N_2} = 2.3 \times 10^{29 \pm 0.2} T^{-3.5} \exp(-113200/T), \quad (3.2-11)$$

$$k_d^N = 8.5 \times 10^{25 \pm 0.2} T^{-2.5} \exp(-113200/T), \quad (3.2-12)$$

($\text{cm}^3 \text{mole}^{-1} \text{sec}^{-1}$) as the best fit over the whole temperature range of the present results. The highest temperature after vibrational equilibration is 19500K, but measurements can only be taken up to 14000K, and the lower limit is 6000K (see Figure 3.1). The approach to equilibrium is also shown in Figure 3.4. The quality of agreement between calculations and experiment is typical of the whole set of results, so that, within the accuracy of the results, the linear rate law, which is assumed throughout, is confirmed for α 's up to 0.5.

If the present experiments are used to find a single overall rate by assuming that N_2 and N are equally effective as collision partners, this total rate can be used together with 3.2-3 and 3.2-11 to deduce k_d^N . The low temperature peaks in the recombination rate coefficient, which is approximately proportional to the pre-exponential factor (CT^{-n}), observed in hydrogen results by Hurle et al. (1969), using this method, do not occur when this method is applied to

the present results.

The rate measurements here are compared with those of previous authors in Figure 3.5 in the form of a logarithmic plot of pre-exponential factor against temperature. Regions where the error margins of different authors overlap are shaded and labelled by the number of authors who agree in the temperature range. The areas of complete agreement are seen to be few and small, and lie on a slope representing a fairly high value of n in both reactions. If the error in the value of the C 's, see 3.2-11 and 12, were entirely accommodated by an error in n it would be $n_1 = 3.5 \pm 0.9$ and $n_2 = 2.5 \pm 1.2$. Thus the error margins on the temperature dependence of the pre-exponential factors according to Hanson and Baganoff (1972) (given as $n_1 = 4.5 \pm 1$, $n_2 = 2.5 \pm 1$) and the present results overlap considerably, while they overlap with Appleton et al. (1968) only for n_2 ($n_1 = 1.6 \pm 0.9$, $n_2 = 1.6 \pm 0.9$, errors estimated from Appleton's scatter). The magnitude of the present results also overlap the results Hanson and Baganoff (1972) throughout their common temperature range. The same is true for the present results and those of Appleton et al. (1968) for all but reaction 3.2-1 at their lowest temperatures. The adjusted $C_2 T^{-n_2}$ value of Allen et al. (1962) is $2 \times 10^{16} \text{ cm}^3 \text{ mole}^{-1} \text{ sec}^{-1}$, at 6400K, which agrees with present results.

The confirmation of Hanson and Baganoff's (1972) strong pre-exponential temperature dependence by the results here suggests that the high n -values are not associated with the difference in the methods of obtaining the data. Common points between the two sets of results are the method of data reduction, the absence of dilutants and the large temperature

ranges covered. The second common point suggests that the high n -values may be associated with the effect of V-V transitions as suggested by Kiefer (1972) for O_2 .

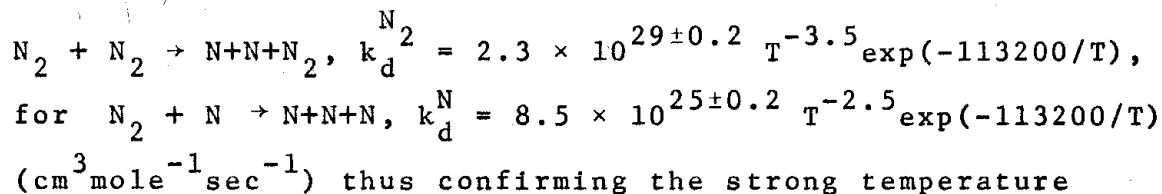
If the non-preferential coupling model of Treanor and Marrone (1962) is used in NSHOCK to analyse the data then k_d^N and $1.3k_d^N$ are found to fit the profiles. At the highest temperatures some form of coupling would be expected (see sections 1.2.2 and 2.4.1) and so a coupling model should be more valid. The non-preferential coupling model depends upon the probability of dissociation from a vibrational energy level being exponentially dependent on the energy needed to dissociate from that and there is some justification for this assumption (Tregay, Valance and MacLean 1972). The preferential model of Marrone and Treanor (1963) may be more realistic but it uses an empirical constant. Both models use the incorrect assumption that the upper levels are in a Boltzmann distribution at the vibrational temperature. A more sophisticated coupling model is probably needed for meaningful rate extrapolations above 14000K.

The induction distances, calculated using Hornung (1972a), for the three shocks in Figure 3.4 are 0.085, 0.037 and 0.016mm in order of increasing shock speed. The present results are unable to resolve these small distances. Experiments at lower densities are needed to observe this phenomena but the fringe shift will also be reduced. The laser schlieren technique of Breshears, Bird and Kiefer (1971) could be used at these lower densities.

3.2.4 Summary

Time-resolved optical interferometry of the relaxation region after the primary shock wave in the free-piston shock

tube DDT is used to measure the dissociation rate of N_2 by N_2 and N without inert gas dilution. The results cover a temperature range of 6000-14000K and give for



dependence of the pre-exponential factor reported by Hanson and Baganoff (1972). The induction time, observed by Horning (1972a), is too small to be resolved.

3.3 T2 Shock Tunnel Experiments

Experimental results on the vibrational de-excitation rate of nitrogen are of interest in gas dynamic lasers (CO-N_2 and $\text{CO}_2\text{-N}_2$) and in recombining nitrogen nozzle flow (see section 3.4). The Landau-Teller model of vibrational relaxation implies that the vibrational de-excitation rate of N_2 is the same as the excitation rate (see section 1.2.1). However Hurle, Russo and Hall (1964), using the SLR technique in a shock tunnel, showed that the de-excitation rate for N_2 was faster, i.e. $\phi > 1$. Since then a number of measurements have been made for ϕ leading to a value of 5 or less (see section 1.2.1 and 2.3.2 for a summary). With the exception of Nagamatsu and Sheer (1965), who used static pressure measurements, the techniques for measuring ϕ were essentially optical. This means that the value of ϕ corresponds to the vibrational "temperature" relaxation rate rather than the vibrational energy de-excitation rate (Hurle 1971). The value $\phi \sim 1$ found by Nagamatsu and Sheer (1965) corresponds to the vibrational energy de-excitation rate. Unfortunately the static pressure technique is relatively insensitive to vibrational relaxation (Rich and Treanor 1970 and Hurle 1971)

as well as being a difficult measurement to make, considering all the corrections that usually have to be made (Duffy 1965). Thus, there still appears to be a need to measure the vibrational energy de-excitation rate at conditions up to significant chemical relaxation, at least to confirm Nagamitsu and Sheer's (1965) results.

Since recombining nitrogen flows will consist of mixtures of N_2 and N, the vibrational relaxation rate of N_2 by collision with N could be important. A brief discussion in section 1.2.1 suggested that, while the relaxation rate of O_2 by O is 2-3 orders of magnitude faster than O_2 by O_2 (Kiefer and Lutz 1967 and Breen et al. 1973a), the N_2 by N relaxation rate should not be greatly different from that of N_2 by N_2 . This suggestion can only be tested by experiment. Borrell (1972) attempted to measure this relaxation rate behind shock waves in mixtures of CO, N_2 and N. The N (~ 0.002 mole fraction) was produced in the shock tube by a RF discharge. The results of this work appear to be unpublished. Another source of providing N_2 and N mixtures is the frozen nozzle flow of a free-piston shock tunnel.

The aim of this section (3.3) is to obtain nitrogen vibrational relaxation rate measurements in the nozzle expansion of the free-piston shock tunnel T2. This is done by placing a flat plate at incidence to the flow. At low incidence, the wedge shock is straight so that a technique similar to that of Stalker and McIntosh (1973) can be used to measure the frozen vibrational energy and thus the vibrational de-excitation rate along the nozzle. At higher incidence the relaxation causes the shock to become curved so that the

vibrational excitation rates of nitrogen can be investigated by the shock curvature technique. The shock shape and density field are determined by optical interferometry. The nozzle reservoir pressure and temperature ranges are 150 to 245 atm and 3000 to 9000K, respectively.

3.3.1 Relaxation Rate Model and Numerical Calculations

The nozzle expansion computer program of Lordi et al. (1966) (NENZF) is used to calculate the flow from the specified reservoir or stagnation conditions. The stagnation conditions are found using the computer program of McIntosh (1970) (ESTC), which assumes an isentropic expansion or compression, from the reflected shock conditions, to the measured stagnation pressure. This assumption, successfully used by Copper (1964), ceases to be realistic if there are effects such as mixing of the shock tube boundary-layer into the test gas by shock reflection (Bull and Edwards 1968), and radiative energy loss (Hornung and Sandeman 1964).

The Landau-Teller rate equation (Eq. 2.6-32) is used to calculate the sudden freeze criterion (Eq. 2.6-36) in NENZF, with the value of τ_v given by Millikan and White (1963a) and Appleton (1967). The values of $k_d^{N_2}$ and k_d^N are those of Appleton, Steinberg and Liquornik (1968) because extrapolation of recombination rates, deduced from the dissociation rates measured in section 3.2, provide poor agreement with room temperature experiments (see Shui, Appleton and Keck 1970 for examples). For mixtures of N_2 and N , the total vibrational relaxation time, τ_v , is given by

$$(1+\alpha)/\tau_v = (1-\alpha)/\tau_v^{N_2} + 2\alpha/\tau_v^N \quad (3.3-1)$$

where α is the atom mass fraction.

If the shock wave attached to the wedge is straight and vibration is in equilibrium behind it (chemistry being frozen) then the free-stream frozen vibrational energy, $e_{v\infty}$, can be measured. This is done by comparing the measured shock angle, β , to the theoretical values calculated from the free-stream conditions found by NENZF. Thus the vibrational de-excitation rate of N_2 can be deduced because the value of $e_{v\infty}$ is determined by τ_v , through the sudden freeze criterion.

The theoretical value of β is found using Equations 2.6-37, 38, 40 and 42 and the relation 2.6-24. From these equations it is seen that β is a function of wedge angle θ , static pressure p_∞ , density ρ_∞ , flow velocity u_∞ , atom mass fraction α_∞ and $e_{v\infty}$. Both static pressure and shock angle measurements are usually made at large area ratios (A/A^* , where A^* is the cross-sectional area of the throat) where α_∞ and $e_{v\infty}$ are effectively constant. This means that, when p_∞ is small and corrections to it are of the same order, the shock angle becomes relatively even better at determining $e_{v\infty}$, through Equation 2.6-40. The ideal position for the wedge appears to be at the largest area ratio possible but this is not the case because the densities would be too low to guarantee vibrational equilibrium behind the shock. Despite this restriction, the measurement of shock angle will be seen, in section 3.3.3.1 to determine the vibrational de-excitation rate at least as accurately as static pressure measurements.

For the study of vibrational relaxation in the wedge flow the shock curvature and fringe shift behind the shock are used. The theoretical shock curvature and flow field are

calculated by the nonequilibrium method of characteristics computer program of Kewley (1974) (NMOCW). The fringe shift is found from Equation 3.2-6.

3.3.2 Experiment

The free-piston shock tunnel known as T2 has been previously described by Stalker (1967). The tube is 2m long, with a 2.1cm diameter, followed by a conical nozzle that has an included angle of 15° and an exit diameter of 7.6cm. The nozzle throat diameter is 0.635cm. The tunnel is operated for the experiments here at three different volumetric compression ratios ($\lambda_p = 37, 20$ and 14) and diaphragm burst pressures ($p_b = 6800$ psi, 3600 psi and 1700 psi), with helium as the driver gas. Another operating condition is provided by using argon as the driver gas with $\lambda_p = 37$ and $p_b = 6800$ psi.

Two thermocouple gauges, 96.5cm apart, are used for shock timing. These consisted of two thermoelectric metal rods, chromel and alumel, roughly 2mm wide and 1mm thick separated by a layer of insulating material approximately 0.02mm thick. At the gauge surface, the thermocouple junction is made by filing in one direction across the exposed ends of the metal until good electrical contact is made (see Stalker 1974). The shock speed is measured to an accuracy of between 1 and 2 percent. However since only two gauges are used the attenuation is unknown. Some estimate is possible for the lowest speeds, where attenuation is more important, by comparing the measured reflected shock pressure with theory. This leads to a maximum reduction of shock speed of 10% for the lowest shock speed used ($\sim 2\text{km sec}^{-1}$). The ensuing error

in the stagnation temperature (taken to be the value for a 5% reduction) is $\pm 300\text{K}$. This error is very large compared to that in experiments by Hurle et al. (1964) and von Rosenberg et al. (1971) but it must be remembered that the range of present stagnation temperatures (nearly 6000K) is nearly 2.5 times larger than these authors' ranges. The shock speeds for particular initial pressures and tunnel operating conditions are shown in Figure 3.6.

The reservoir or stagnation pressure is measured with an S.L.M. type HPZ-14 piezoelectric pressure transducer located in the shock tube wall, 1.78cm from the end. The measured stagnation pressure is approximately constant over about 100 μsec for each of the shock tunnel operating conditions and is between 150 and 245 atm, with an accuracy of $\pm 10\%$.

To determine the effect of boundary-layer growth on the nozzle expansion, the Pitot pressure is measured at different axial positions and compared with theoretical values for various inviscid conical nozzle flows. The effective nozzle shape is that which gives agreement between the theoretical and measured Pitot pressure. The theoretical Pitot pressure is given by

$$P'_0 = p_\infty + \rho_\infty u^2 (1 - \frac{1}{2}(\rho_\infty / \rho_s)) \quad (3.3-2)$$

where ρ_s is the density at the stagnation point of the Pitot probe; usually p_∞ can be neglected and the density ratio is between 0.17 and 0.10. The Pitot pressure probe consists of a Kistler 603H piezoelectric pressure transducer housed in a brass mounting with a type 556c impedance converter.

Figure 3.7 shows a picture of the probe and the results of an axial Pitot pressure survey. The effective nozzle included

angle is taken to be $14 \pm 0.5^\circ$ when calculating the free-stream conditions of this case (D2), where the stagnation conditions are $T_0 = 4400\text{K}$ and $P_0 = 227\text{ atm}$. For the present range of experiments the effective nozzle angle varies from 13 to 14 degrees. The eleven nozzle flows used for the experiments are summarised in the following Table 3.1. The initial conditions are found in Figure 3.6. The high enthalpy conditions (A1 - A4, see Figure 3.6) are not used for the relaxation rate measurements.

Once the nozzle stagnation conditions and the effective, inviscid nozzle shapes are found, there still remains the problem of defining the test time during which flow over a wedge is to be studied. The test time is limited by the nozzle starting processes (Smith 1966) and driver gas contamination of the nitrogen. One method of finding the useful test time is the technique developed at ANU by Stalker and McIntosh (1973). They took schlieren photographs, using a 2 μsec duration light source, of flow over a 35° wedge at various times after shock reflection occurred in the shock tube. They showed that the shock angle rose to a steady value for a time and then rose again. This second rise was interpreted as being caused by driver gas contamination of the flow. However, it is possible that in their dissociated flows the contamination by a monatomic driver gas is compensated by the reduction in the proportion of dissociated molecules, giving no change in shock angle, and therefore this method may be overestimating the test time. This method is used here, in conjunction with qualitative static pressure measurements of the flow over a flat plate, to determine the test time.

Table 3.1: T2 nozzle stagnation and free-stream (at 26cm and $\phi = 1$) conditions.

	A5	B1	B2	B3	C1	C2	C3	C4	D1	D2	D3
P_o, atm	245	203	210	223	150	160	170	175	227	227	227
T_o, K	8900	9100	8400	7450	7800	6450	5200	4500	5650	4400	3700
Nozzle angle, degrees	13.5	13.5	13.5	13.5	13.0	13.0	13.0	13.0	14.0	14.0	14.0
α_∞	0.079	0.115	0.054	0.015	0.038	0.008	0	0	0	0	0
$\rho_\infty \times 10^5, \text{gm cm}^{-3}$	1.5	1.2	1.4	2.0	1.3	1.8	2.4	3.0	2.5	3.5	4.2
$u_\infty, \text{kms}^{-1}$	5.3	5.5	5.0	4.3	4.6	3.8	3.3	3.1	3.5	3.0	2.8
T_∞, K	1820	1890	1540	1120	1280	830	600	500	640	460	370
$p_\infty \times 10^{-4}, \text{dyn cm}^{-2}$	8.6	7.2	6.9	6.6	5.0	4.6	4.3	4.5	4.8	4.8	4.6
M_∞	5.8	5.8	6.0	6.3	6.1	6.5	6.7	6.7	6.8	6.9	7.0
T_v, K	3760	3840	3570	3190	3490	3020	2710	2500	2740	2450	2300

The static pressure is measured using the flat-plate, pressure transducer holder, developed by Ebrahim (1975), and successfully used for chemically reacting carbon dioxide nozzle flows in T2 (Ebrahim and Hornung 1975). For the present experiments, the time variation of the static pressure indicates the onset of He driver gas contamination in the flow. Figure 3.8 shows that the static pressure rises (with a response time of 50 μsec) to a peak, then falls away to a steady value. Interferograms of flow over a wedge, taken at times corresponding to this steady static pressure, give shock angles at least 2° higher than theoretical predictions. For interferograms taken at the time of peak static pressure, the shock angles are close to theoretical predictions (see the next section). Thus the drop in static pressure is interpreted

as the end of the test time. However, when an Ar driver gas is used, the static pressure rises to a reasonably constant value and remains at that value for 700 μ sec. This could be interpreted as the useable test time but shock angle measurements show that this is not the case (see the next section).

The Carl Zeiss Mach-Zehnder interferometer, used in section 3.2, is used to obtain interferograms of the flow over a sharp flat plate, 57mm wide and 63mm long, at incidence to the flow. The tip of the plate is as close as possible to the centre of the flow. A $5100\overset{\circ}{\text{A}}$ interference filter of $40\overset{\circ}{\text{A}}$ bandwidth is introduced into the system, on the downbeam side of the interferometer, in front of a Hasselblad camera loaded with Ilford HP4 film. The light source is a Hadland 2 μ sec Xenon flash lamp HL.101.

The shock tube and dump tank are evacuated to a pressure of less than 10^{-2} torr. The shock tube is then filled with nitrogen and evacuated again in order to reduce contamination from the air in the room. The lowest filling pressure for the relaxation experiments is 101.5 torr.

3.3.3 Results

3.3.3.1 Shock Angle Measurements

The measured shock angles on the flat plate at 35° , 39° and 41° incidence to the flow, for the range of stagnation temperature T_0 , are shown in Figures 3.9, 10 and 11. The time, after shock reflection, of the interferograms, used to measure the shock angle, is also given. The theoretical values of the shock angle are also plotted. These are found from the free-stream conditions given by nozzle flow

calculations for various values of vibrational de-excitation rate. The variation of theoretical shock angle with T_0 is reasonably smooth, despite the position of the plate being constant, 26cm from the throat, and thus the area ratio depending upon the effective inviscid nozzle shape. This is to be expected, following the qualitative discussion given in section 3.3.1, and is quite a contrast to the much greater sensitivity of static pressure measurements on the area ratio (see Duffy 1965 and Nagamatsu and Sheer 1965). Unfortunately before any comparison can be made between theory and experiment, there are two corrections that need to be considered. The divergence of the free-stream causes the shock angle to be reduced from the value corresponding to a uniform flow. The growth of a boundary-layer on the wedge causes the effective, inviscid wedge angle to be larger. (Both these corrections were necessary to adjust the measured shock angles for the experiments of Stalker and McIntosh (1973)). This type of correction is the main disadvantage of the wedge-shock-angle type of experiment.

Using the theory of Hall (1963) the effect of flow divergence is found to cause a reduction of between 0.1° and 0.4° ($\theta = 35^\circ$ to 41°) in the shock angle at 5mm from the wedge tip, for the range of experiments. The boundary-layer correction is found by obtaining the slope of the displacement thickness for a frozen zero-pressure-gradient boundary-layer with a Prandtl number and Lewis number of one. The reference-enthalpy method (Hayes and Probstein 1959 p.296) is used to find the reference Reynolds number. This method of calculating the displacement thickness was used by Stalker and McIntosh (1973). These assumptions have also been

successful in calculations of the boundary-layer thickness on a flat plate in air, in the shock tunnel T3 (Baird 1972). The viscosity of N_2 and N mixtures is found by the method given in Dorrance (1962 p.277). The effect of the displacement thickness on the wedge angle is an addition of 0.4° , at 5mm from the wedge tip, for stagnation temperatures up to 6500K which reduces to 0.15° at 9100K. The reference Reynolds number, R_e^* , varies from 5.4×10^4 to 1.2×10^4 . This type of calculation is valid if there is only a weak interaction between the boundary-layer and shock wave. This is true if the parameter, $\bar{\chi} = M_s^3 / (R_e^*)^{1/2}$ is less than one (Dorrance 1962 p.147). The maximum value for $\bar{\chi}$ at 5mm from the wedge tip is 0.09 for the present experiments.

These corrections applied to the results show that the vibrational de-excitation rate is equal to the excitation rate, within an accuracy of a factor of 10 ($\frac{1}{10} < \phi < 10$). The experiments here are in agreement with the theoretical calculations in section 2.3.2, for the experiments of Hurle, Russo and Hall (1964), which give a value for the vibrational de-excitation rate of nitrogen not greater than ten times the excitation rate. To achieve a more accurate measurement of the vibrational de-excitation rate, using the present method, it would be necessary to reduce the size of the flow divergence and the boundary-layer displacement thickness corrections. This could be done by using a longer conical or contoured nozzle but, at the same time, using higher Reynolds numbers. This condition can be fulfilled, if a larger nozzle throat and either a smaller area ratio for the wedge position or, preferably, higher stagnation pressures are used.

3.3.3.2 Shock Curvature Measurements.

As shown in section 2.6.4.1, the shock curvature is directly proportional to the relaxation rate behind the shock over a wedge and therefore can, in principle, be used to measure the relaxation rate. Here the shock curvature is used to measure the N_2 by N_2 and N_2 by N vibrational excitation rate. This technique for measuring relaxation rates from the experimental shock curvature on a wedge has been shown to work for dissociation (see section 3.4.3) and has also been used by Smith and Wegener of Yale University (in a study available only as an internal report) to measure evaporation rates in flow over a wedge. This latter work is also reported in Becker (1972 p.187).

The experimental shock curvature is given by

$$\kappa = \frac{f''(x)}{(1+(f'(x))^2)^{3/2}} \quad , \quad (3.3-3)$$

where $f(x)$ is the polynomial, found from a polynomial regression program, for the position of the shock and x is the distance along the wedge. The experimental shock curvature obtained from the two interferograms of flow over the inclined flat plate presented in Figure 3.12 and six others, is plotted against the shock angle for the nozzle reservoir conditions A5, B2, C1 and B3 in Figures 3.13(a-d). Also plotted are theoretical calculations of the shock curvature obtained from NMOCW, with the vibrational excitation rate of Millikan and White (1963a) and Appleton (1967), for both N_2 - N_2 and N_2 - N collisions. The values of the free-stream atom mass fractions are given in Table 3.1. If the vibrational excitation rate of N_2 by N causes the total vibrational excitation rate to increase by a factor of 4 then τ_v^N (found using Equation 3.3-1)

will be equal to $\tau_v^{N_2}/21.5$ for A5, $\tau_v^{N_2}/30.3$ for B2, $\tau_v^{N_2}/39.2$ for C1 and $\tau_v^{N_2}/102.5$ for B3. The experimental results show that the excitation rate of N_2 by N is probably less than 50 times faster than the N_2 by N_2 rate, if the shock curvature is due only to vibrational relaxation over the wedge. The range of temperature is between 10300K and 7000K. However other causes contributing to shock curvature must be considered.

One of these is the effect of the conically divergent free-stream. Again, the theory of Hall (1963) is used to calculate this correction for the experimental cases. The error incurred in neglecting the divergence effect in the experiments here is always less than 0.1 cm^{-1} and 0.04 cm^{-1} , for wedge angles of 41° and 39° , respectively. Another contribution to the shock curvature is the boundary-layer growth on the wedge. The $\partial\xi/\partial s$ -term in Equation 2.6-45 is changed from zero (being the flat plate curvature) to the streamline curvature caused by boundary-layer growth. $\partial\xi/\partial s$ is made equal to the rate of change of displacement thickness slope along the wedge. The increase in shock curvature is about 0.01 cm^{-1} at 1mm from the leading edge. Thus the importance of the two effects is reversed from that for the shock angle measurements. These two corrections, plus uncertainties in α_∞ and ϕ , make high precision measurements of the N_2 by N relaxation rate from the present experimental shock curvatures rather optimistic.

Figure 3.12 also shows the calculated flow field, neglecting the flow divergence and the boundary-layer, for a wedge angle of 41° with the nozzle conditions of B3. The contours of fringe shift, relative to the free-stream, are

plotted over the actual characteristics mesh points obtained from NMOCW. The excitation rate, for both N_2-N_2 and N_2-N collisions, is that given by Millikan and White (1963a). The fringe contour of 2.4 shows up the effect of the entropy layer found by Sedney, South and Gerber (1962). The distance between the shock wave and wedge compares favourably with experiment.

From the results presented in Figure 3.13 it can be seen that, although these experiments are not of high precision, they indicate that the N_2 by N vibrational excitation rate is less than about 50 times faster than the N_2 by N_2 rate. However, this result assumes that the non-Boltzmann vibrational population distribution of the N_2 in the free-stream (see section 2.3.1) has a negligible effect on the validity of the Landau-Teller vibrational relaxation equation behind the shock. One expects that this would be the case if there is no large population inversion, for example $X_{35} \sim X_5$, in the upper levels. The highest value of Y , for the shock curvature measurements would be 3760K, assuming $\phi = 1$, with the lowest T_∞ being 1120K. Figure 2.2 shows that, for these value of Y and T , a large population inversion is not expected.

3.3.4 Summary

Experiments in the small free-piston shock tunnel T2 show that the vibrational de-excitation rate of nitrogen is equal to the excitation rate of Millikan and White (1963a), within a factor of ten, and that the vibrational excitation rate of N_2 by N is less than about 50 times the excitation rate of N_2 by N_2 , over a temperature range 7000-10300K. Both results are found by examining the flow over a flat plate, inclined to the flow, with optical interferometry. The effects

of flow divergence and boundary-layer growth on the wedge are shown to be significant corrections, more so for the shock angle measurements than for the shock curvature measurements. Thus, more precise experiments require that both effects are reduced.

The wedge-shock-angle type of experiment (Stalker and McIntosh 1973) has been developed, in section 3.3, to measure the frozen vibrational energy of N_2 in the flow and thus the vibrational de-excitation rate of N_2 in the nozzle expansion. The wedge-shock-curvature experiments of section 3.4.3 and Kewley and Hornung (1974b) have been extended to studying vibrational excitation behind a shock.

3.4 T3 Shock Tunnel Experiments

Experimental studies of chemically relaxing nozzle flows of diatomic gases are difficult to perform, and the results have generally not achieved sufficient accuracy to make a critical assessment of the relaxation rate models (Bray 1970b). Previous experiments by Nagamatsu and Sheer (1965), for N_2 , and Russo, Hall and Lordi (1966), for H_2 -Ar, demonstrate that more accurate diagnostic techniques than static pressure measurements are required, before a realistic comparison between theories of the type presented in Chapter 2, and experiments, in the simplest of chemically relaxing flows, can be made. The best technique is one that measures the species concentration in the flow; ideally the flow should be such that significant differences in the species concentration occur between equilibrium and frozen flow calculations. Thus experiments accurately measuring the species concentration of an undiluted diatomic gas recombining in the nozzle flow would provide the basis for comparison with the theory given in

Chapter 2. Experiments of this type have been made in nitrogen using the large free-piston shock tunnel T3 by Crane (1975) at A.N.U. His results, obtained with a mass-spectrometer, are analysed in section 3.4.3.1.

Although a large number of numerical and analytical studies of nonequilibrium hypersonic flow over bodies have been made, actual experiments are scarce. Some chemically relaxing flows of undiluted oxygen over a cone have been studied by Spurk and Bartos (1966) and Spurk (1970) in an expansion tube. The first experiments in T3 of nitrogen flow over circular cylinders (Hornung 1971, 1972a and 1972b) demonstrated that nonequilibrium dissociating flows of nitrogen over bodies can be obtained. These experiments showed the existence of an induction time before appreciable dissociation occurs but were unable to resolve between the reaction rates of Cary (1965) and Appleton, Steinberg and Liquornik (1968), particularly just behind the shock. On the other hand, it is anticipated that dissociating nitrogen flow over a wedge would be more sensitive to the initial reaction rates behind the shock, on the basis of theoretical studies by Sedney (1961) and Spurk, Gerber and Sedney (1966). Thus an experimental investigation of relaxing nitrogen flow over a wedge was undertaken, with the help of Dr H.G. Hornung, in 1971. Preliminary calculations (Kewley 1971) showed that the initial shock curvature at the tip of the wedge agreed with expected values at a stagnation enthalpy of $2.34 \times 10^{11} \text{ cm}^2 \text{ s}^{-2}$, but as the stagnation enthalpy increased the experimental values fell to nearly an order of magnitude below the theoretical initial shock curvature. The reason for this discrepancy was not understood and subsequently prompted the work presented in this

thesis.

The dissociation rates of nitrogen in a shock tube are investigated in section 3.2 and found to be between the values given by Hanson and Baganoff (1972) and Appleton et al. (1968), thus the discrepancy is not explained by incorrect values of initial dissociation rate. Another possibility, that the free-stream α_∞ could be wrong due to vibration-recombination coupling invalidating the rate-quotient law, is found, in section 2.4.3, to be unlikely. This, and the demonstration in section 2.4.3, that the vibrational energy de-excitation rate in a recombining flow is adequately described by the Landau-Teller equation, and combined with the experiments in section 3.3, leads one to conclude that the conventional method of calculation for recombining nozzle flows (Lordi et al. 1966 and section 2.6.3) can be discounted as the source of the discrepancy. The effect of vibration-dissociation coupling is uncertain at present. Part of the experimental study of the nitrogen nozzle flow by Crane (1975) was to measure the helium concentration relative to the total nitrogen concentration. His experiments show significant He contamination earlier in the flow than had been expected, particularly at high enthalpy. This contamination, coming from the driver gas, and the resulting reduction in α_∞ is included in the calculations for the dissociating nitrogen flow over wedges, in section 3.4.3.3.

The work presented in this section (3.4) aims to demonstrate the feasibility of obtaining the dissociation rate of nitrogen at high temperatures by measuring the curvature of the shock at and near the tip of the wedge. The most common method of measuring dissociation rates is to study the density

rise after a normal shock in a shock tube. At high shock speeds, and consequently at high temperatures it is difficult to measure the initial rate accurately by this method (see section 3.2.3), while the shock curvature technique can be expected to give good results at high temperatures. Another interesting feature of the curvature technique is that the free-stream degree of dissociation may be varied in the shock tunnel, so that, ideally, the relative efficiency of atomic and molecular nitrogen as a collision partner in dissociation can be measured. The results of an inverse technique (Garr and Marrone 1963), which calculates the flow field by integrating towards the body from a measured shock, and the nonequilibrium method of characteristics (Kewley 1974) are both compared with the experimental flow field over a wedge, obtained by optical interferometry.

In addition, the experimental results of Crane (1975) for α_{∞} and He contamination are examined. The conclusions of this examination are used for the free-stream condition calculations necessary to investigate flows over a wedge.

3.4.1 Relaxation Rate Model and Numerical Calculations

The free-stream conditions in the nozzle flow are calculated using the nonequilibrium nozzle flow program of Lordi et al. (1966) (NENZF), as is done in section 3.3. At the high temperatures of these nozzle flows, the effect of ionization of the molecules and atoms is accounted for by including the seven reactions recommended in Dunn and Lordi (1970) and used in section 3.2. The electron temperature is taken to be equal to the translational temperature. Again, the nozzle reservoir or stagnation conditions are found by isentropically expanding or compressing the calculated reflected

shock conditions, determined by the initial pressure and incident shock speed, to the measured stagnation pressure.

If the attached shock on the wedge is straight then it can be calculated using Equations 2.6-37, 38, 39, 40 and 42, assuming that vibration is in equilibrium and that dissociation is frozen. As mentioned previously, agreement between theoretical and experimental shock angles does not imply that the free-stream atom mass fraction, α_∞ , is determined. A reduction in α_∞ can be compensated by contamination by a monatomic gas. As in section 3.3.3.1, the vibrational energy de-excitation rate of nitrogen can be deduced from the measured shock angles but for the present experiments the resolution between rates is not very good.

The initial shock curvature, at the tip of the wedge, is calculated, for a particular dissociation rate, from Equation 2.6-45, once the conditions just behind the shock are found. If the wedge is flat, it is seen that the initial shock curvature is directly proportional to the dissociation rate. The variation of shock curvature with shock angle is also a function of dissociation rate but it is necessary to use the method of characteristics calculation (Kewley 1974) (NMOCW) to relate this variation to the dissociation rate. The total chemical reaction rate is assumed to be given by the linear rate law for both the nozzle flow calculation and the calculated flow behind the oblique shock.

For flows consisting of mixtures of N_2 , N and He, the fringe-shift Equation 3.2-6 must be generalised. A general expression is given by

$$f = \sum_i K_i W_i (c_i \rho - c_{i\infty} \rho_\infty), \quad (3.4-1)$$

where K_i is the Gladstone-Dale constant, in $\text{cm}^3 \text{g}^{-1}$, W_i is the molecular weight and c_i is the concentration in mole (g of mixture)⁻¹ of the species i . The Gladstone-Dale constants for N_2 , N and He are 0.24, 0.31 and $0.20 \text{ cm}^3 \text{g}^{-1}$, respectively.

3.4.2 Experiment

Most of the experiments to be analysed in section 3.4 have already been presented in Kewley(1971) and Crane(1975). Some further wedge experiments in nitrogen, using the present setup, have been performed by Pratt and Kewley (1974) as part of a study of reacting air flows.

The large free-piston shock tunnel T3 and its instrumentation has been described in more detail elsewhere (Stalker 1972 and 1974). The 7.6cm diameter shock tube is 6m long and is followed by a conical nozzle of included angle 15° and exit diameter 20.3cm; the throat diameter is 1.27cm. For the experiments studied here the volumetric compression ratio for the free-piston compression is 60 and the driver gas is helium. The stagnation pressure is measured with a Kistler 6201 quartz-crystal pressure transducer, and is about 220 atm. The effective nozzle area ratio, for the wedge experiments (260), has been found by matching the calculated and experimental Pitot pressures (Hornung 1972b).

The Carl Zeiss Mach-Zehnder interferometer, used previously in sections 3.2 and 3, has an exploding wire as a light source (see section 3.2.2). A band-pass filter of $5330 \pm 100\text{\AA}$ is placed in front of the Hasselblad camera. The interferograms of flow over a sharp flat plate, 15.4cm wide and 14cm long, are taken on Ilford HP4 film and developed in Kodak DK60A.

Details of the mass-spectrometer experiments analysed here are given in Crane (1975). The exit diameter of the nozzle is 30.5cm. The area ratio at the sampling skimmer position, without any boundary-layer correction, is 830 and, since the free-stream concentrations are theoretically frozen at area ratios greater than 200, this is the area ratio used in the calculations.

The shock tube is evacuated to a pressure of less than 10^{-3} torr and is filled with nitrogen to a minimum pressure of 12.7 torr, for the mass-spectrometer experiments, and 50.7 torr, for the wedge experiments. The dump tank is evacuated to a pressure of less than 10^{-1} torr.

3.4.3 Results

The experimental results, for the relative free-stream concentrations of N_2 and N, of Crane (1975) are analysed, with He contamination included. The conclusions are then applied to the wedge experiments of Kewley (1971), which have previously been presented with no helium contamination by Kewley and Hornung (1974b). The experimental shock curvatures are compared with the theoretical shock curvatures, at and near the tip, calculated by NMOCW.

3.4.3.1 Analysis of Mass-Spectrometer Results obtained by Crane (1975)

The measured relative species concentrations of N_2 , N and He are given against initial shock tube pressure in Figure 3.14. The experimental measurements of N_2 and N concentrations are made during two separate runs and consequently this is a major contribution to the size of the error bars. The theoretical values of α_∞ , for the supposed nozzle stagnation conditions, are calculated from NENZF using

the shock-tube-determined rates of Appleton et al. (1968). The results for the 8 in. case show no He contamination and are also the most sensitive to variations in the recombination rate. To get agreement with α_∞ , within the experimental errors, the rate has to be decreased by a factor of 2, and to agree with the mean value of α_∞ , by a factor of 5.

Following a suggestion by Dr R.J. Stalker, it is noted that the free-stream velocity measurements of McIntosh (1971) and Stalker and McIntosh (1973), in air, agree within an accuracy of $\pm 5\%$, with the theoretical value calculated from NENZF. However, if the measured He contamination is included in the nozzle calculations, the stagnation pressure and temperature being unchanged, the free-stream velocity, u_∞ , is increased by 7.5% and 15.3%, for 2 and 0.5 in. of Hg of N_2 in the shock tube, respectively. Therefore to get agreement with the supposed-correct value of u_∞ , the stagnation temperature is reduced until agreement is reached. The results of calculations for α_∞ , plus the new value of T_0 obtained by this method are given in Figure 3.14. The recombination rate of N_2 by He (k_r^{He}) is taken to be $k_r^{N_2}/3.7$, based on k_d^{Ne} measurements by Cary (1965). The new values of α_∞ are much closer to the experimental results. The reason for the improved agreement is that the α in the stagnation region, and consequently α_∞ , is reduced. When the upper limit in the value of r , defined as $[He]/([N_2]+[N])$, is used in the calculations for the 1 in. and 2 in. conditions, agreement is improved but the theoretical values for α_∞ are still larger. It becomes apparent that free-stream velocity measurements are vital for any experiments where He contamination is expected.

The experimental results, for α_∞ , of Crane (1975) agree reasonably well with theoretical calculations using NENZF, with the reaction rates of Appleton et al. (1968) and the measured He contamination. The calculations are dependent on knowing accurately the free-stream velocity. However the "success" of the present calculations is made the basis of calculating the "correct" free-stream conditions for the wedge-flow experiments in the next section, despite the fact that no accurate velocity measurements have been made for these flows.

3.4.3.2 Results with 35 degree Wedges

Before the analysis of shock curvature over a wedge, it is important to examine the case where the shock is effectively straight. As demonstrated in section 3.3.3.1, the shock angle can be used to deduce the free-stream vibrational energy and thus the vibrational de-excitation rate, if there is no appreciable vibration-recombination coupling. The experiments are conducted with initial shock tube pressures of 6, 4, 3 and 2 in. of Hg of N_2 . The calculated stagnation and free-stream conditions, without He contamination, are given in Table 3.2.

Throughout the experimental range, a wedge at 35° incidence produces a virtually straight shock wave with a small curvature at the tip of the higher enthalpy case. For a straight shock, β and θ determine the density ratio ρ_s/ρ_∞ from Equation 2.6-41. From the fringe shift across the shock the density difference $\rho_s - \rho_\infty$ is found. Thus both densities can be determined from an interferogram such as that in Figure 3.15. The error in ρ_∞ from this determination varies from $\pm 6\%$ to $\pm 11\%$, for the I and IV cases, respectively.

Table 3.2: T3 nozzle stagnation and free-stream (at 78cm and $\phi = 1$) conditions

	I		II		III		IV	
p_1 in. of Hg	6		4		3		2	
u_1 , kms ⁻¹	4.98		5.43		5.84		6.23	
$h_0 \times 10^{-11}$, cm ² s ⁻²	2.34	2.31	3.0	2.9	3.4	3.2	4.0	3.7
T_0 , K	9380	9320	10000	9825	10400	10100	10900	10500
P_0 , atm	232	232	228	228	226	226	225	225
α_∞	0.12	0.115	0.20	0.18	0.26	0.22	0.35	0.28
$\rho_\infty \times 10^6$, g cm ⁻³	4.6	4.6	3.9	3.8	3.5	3.4	3.0	3.0
u_∞ , km s ⁻¹	5.8	5.8	6.3	6.3	6.7	6.7	7.1	7.1
T_∞ , K	1530	1450	1730	1500	1810	1510	1900	1490
$p_\infty \times 10^{-4}$, dyn cm ⁻¹	2.4	2.25	2.4	2.13	2.4	2.04	2.3	1.93
M_∞	6.8	7.0	6.7	7.1	6.7	7.1	6.7	7.3
T_v , K	3900	3600	3900	4000	4050	3900	4100	4000
r	0	0.03	0	0.09	0	0.13	0	0.20

This result can then be used with measurements of the free-stream Pitot pressure (Hornung 1972b), which is approximated very closely by $0.95 \rho_\infty u_\infty^2$, to determine the free-stream velocity to within $\pm 8\%$. The agreement with the calculated u_∞ in Table 3.2 is within 3% for I, II and III and 5% in IV. The density ratio ρ_s/ρ_∞ is sensitive to α_∞ and e_{v_∞} , the two nonequilibrium variables of the nozzle flow, but it does not uniquely determine α_∞ because He contamination can compensate the loss of N atoms. The results of shock angle measurements (Kewley 1971) are given in Figure 3.16. The I and IV conditions were repeated several months after the bulk of the experiments were completed. These results provide a measure of the shot-to-shot repeatability of the free-stream conditions. Calculations for various vibrational

de-excitation rates, assuming τ_v^N and τ_v^N to be the same (see section 3.3.3), show that either a value of τ_v , which is 50 times slower than the shock tube value of Millikan and White (1963a), i.e. $\phi = 1/50$, or a value of τ_v , which is the same as the shock tube value, coupled with a boundary-layer displacement effect, is needed to fit the experimental results. The calculated boundary-layer displacement effect (see section 3.3.3.1) gives a correction of at least 0.2° to the wedge angle for these experiments. A simple correction of adding 0.5° is used for the range of results. The flow divergence effect is negligible because the nozzle is 3.5 times longer than that used for T2.

Of course the effects of helium contamination have to be considered because of the unexpected results of Crane (1975). The approach to calculating the free-stream conditions is the same as that given in section 3.4.3.1, with the value of the relative He concentration taken to be the same for the 2 in. (IV) and 4 in. (II) cases and interpolated for the 3 in. (III) and 6 in. (I) cases. The interpolated helium concentration for case I is considered to be pessimistic. The resulting stagnation and nozzle conditions, with He contamination are listed in Table 3.2.

Calculations using these free-stream conditions give values for the shock angle very similar to the results with no He contamination, see Figure 3.16. This lack of difference between the He-contaminated flows and the pure flows explains why Kewley (1971) and Kewley and Hornung (1974b) did not consider this possible contamination more closely. Previously it was thought that the agreement between theory and experiment for u_∞ and β was sufficient to exclude this possibility.

The 35° -wedge results serve to confirm the calculations of the free-stream conditions, excluding α_∞ , which are used to calculate the initial shock curvature.

3.4.3.3 Initial Shock Curvature

Again, causes other than relaxation contributing to shock curvature must be considered. One of these is the effect of the conically divergent free-stream. This effect is discussed in detail by Hall (1963), whose results are used to calculate this correction for each experimental case. The error incurred by neglecting the divergence effect always represents less than 8% of the measured initial curvature. The magnitude of this effect can be observed to be small by performing wedge-flow experiments with similar shock angles under frozen-flow conditions in the same nozzle, by lowering the enthalpy. In such experiments, the shock curvature is observed to be so small that it is not possible to resolve its cause.

Another contribution to the shock curvature is the boundary-layer growth on the wedge, through the $\partial\xi/\partial s$ term in Equation 2.6-45, which is made equal to the rate of change of boundary-layer displacement thickness slope along the wedge. An approximate theoretical calculation of the boundary-layer effect can be made but the simplest way of determining its contribution is to measure the shock curvature at low-wedge-angle ($\theta=35^\circ$), where the boundary-layer is the main cause of shock curvature. This leads to a value of about 0.01 cm^{-1} at 1mm from the leading edge. This is a conservative estimate of the boundary-layer contribution at higher wedge angles, because the boundary-layer thickness and displacement effect decrease as the wedge angle is decreased. It

represents about 3% of the measured initial curvatures at higher angles.

Near the detachment limit, a third contribution arises because the flow downstream of the shock is then subsonic. Consequently, the expansion at the trailing edge of the wedge is able to influence the whole flow field up to the tip, thus curving the shock from the tip to a point opposite the trailing edge, where the flow will have reached sonic speed. The maximum possible change in shock angle owing to this contribution over the length is 0.5° at the free-stream Mach number of present interest.

The experimental shock shape is obtained from the interferograms by measuring at both edges of each fringe, for the first 20 fringes, the distance from the wedge surface to the point where the fringe first registers the density rise at the shock front. These measurements are made to an accuracy of $\pm 0.04\text{mm}$ in the region of interest, which is restricted to a distance of about 1cm from the wedge tip. A least-squares fit to these points then gives the shock shape as a polynomial in distance along the wedge surface, from which the shock-wave curvature κ and angle β may then be calculated as functions of distance along the wedge (see section 3.3.3.2.).

To show the source of the experimental information, Figure 3.17 shows an interferogram corresponding to the case $\theta = 41.5^{\circ}$ of Figure 3.18a. The curvature of the shock as well as the rise in fringe shift between shock and body, corresponding to the density rise due to dissociation, are clearly visible. The rise in fringe shift close to the body indicates the boundary-layer thickness. The kinks in the fringes right on

the body surface are due to an optical effect which is observed when the model is well aligned with the light beam.

To compare the experimental results with theory, the initial curvature is calculated at each tunnel condition for a number of values of β . This is done using the free-stream conditions given in Table 3.2. For the determination of the initial shock curvature from Equation 2.6-45, the dissociation rates of Appleton et al. (1968) and Hanson and Baganoff (1972) are used, because these rates encompass all the other determinations (including section 3.2), and the vibrational energy is assumed to be in equilibrium downstream of the shock. It should be pointed out that the nozzle flow is very insensitive to the recombination rate (see the last section for an example) in comparison with the sensitivity of the shock curvature to the dissociation rate, and that the temperatures involved in the nozzle flow are considerably lower than those behind the wedge shock, so that the choice of rates does not affect the nozzle flow significantly, and the conditions (in the nozzle flow) are within the temperature range where the rates are relatively well known. Similarly, the effect of altering the vibrational de-excitation rate in the nozzle flow from 1/50 of Millikan and White's (1963a) rate to an infinite rate is to alter the initial shock curvature by no more than $\pm 12\%$ in the present range of interest.

The results of the initial shock curvature calculations are plotted in Figures 3.18(a-d), in order of increasing enthalpy, as graphs of initial curvature against shock angle for both the dissociation rates of Appleton et al. (1968) and Hanson and Baganoff (1972), and for pure and He-contaminated nozzle flows. Superimposed on these figures are the curvature-slope traces of some experimental shock waves. It

should be pointed out that each experimental curve represents the $\kappa(\beta)$ trace of the whole of the shock, so that the right-hand end of the trace gives the values of κ and β at the tip of the wedge, whereas the calculated curves represent tip values only. Thus for agreement of experiment with predictions according to previously measured rates, the right-hand (large β) end of the experimental curve should fall on the calculated curve. The error bars indicate the estimated uncertainty in the experimental results from all sources.

At the lowest stagnation enthalpy (Figure 3.18a) the experimental initial shock curvature is seen to be in good agreement with the values predicted by the dissociation rates of Hanson and Baganoff (1972) for the uncontaminated flow but is a factor of three higher for the He-contaminated flow. As mentioned already the amount of helium in the flow, interpolated from the results of Crane (1975), is likely to be an upper bound, and the calculations in the next section appear to confirm that the contamination is much smaller. At the intermediate stagnation enthalpies (Figures 3.18b and c), the experimental curvature is in approximate agreement with the value predicted using the dissociation rates of Appleton et al. (1968), for uncontaminated flow, and the dissociation rates of Hanson and Baganoff (1972), for contaminated flow. Experimental results from Pratt and Kewley (1974), for a case similar to III, are similar to those presented here. For the highest stagnation enthalpy (Figure 3.18d), the experimental curvature is well below the predicted curves for uncontaminated flow but falls between them for contaminated flow. These results indicate that the discrepancy between experiment and theory for the highest stagnation enthalpy

(see Kewley (1971) and Kewley and Hornung (1974b)) is due to helium contamination in the nozzle flow. Because the actual helium concentration and its consequent effect on the atom mass fraction is still uncertain, although it is certainly better known now (Crane 1975), it is considered that deducing new dissociation rate data from all these results is not possible. However the results do show that previous determinations give reasonable agreement between the experimental and theoretical initial shock curvature; the highest temperature behind the shock being 1460K. If there is no helium contamination in the flow, for the lowest enthalpy case, then a more precise analysis of the two shock curvature versus shock angle profiles (Figure 3.18a) can be attempted. This is assumed for the theoretical flow field calculations in the next section.

3.4.3.4 Calculation of the Flow Field

Inverse techniques of calculating supersonic flow fields, in which the shock is assumed to be known and the body shape emerges as part of the solution, are open to criticism because of the question of whether to each shock shape there corresponds a single body shape. This objection disappears if the flow field downstream of the shock wave is supersonic throughout. Thus, an inverse method, in which the flow field is calculated by starting from the measured shock-wave shape, should give the correct body shape and fringe shift distribution, provided that the reaction rates are correct. Of three calculations made with different reaction rates at conditions corresponding to those of Figure 3.17 one is shown in Figure 3.19. The method used is basically that of Garr and Marrone (1963) with modifications as described in

Hornung (1972b). The reaction rates for this calculation are taken from section 3.2. These fall between the rates measured by Appleton et al. (1968) and Hanson and Baganoff (1972) (see Figure 3.5a and b) and therefore predict curvature lying between the two calculated curves of Figure 3.18. An additional refinement of this calculation is that vibrational relaxation is accounted for by a Landau-Teller model with Millikan and White's (1963a) rates. Figure 3.19 gives the calculated fringe shift contours in the region close to the tip. It can be seen that the calculated body shape is indistinguishable from a straight wedge, but the calculated θ is 0.7° larger than the actual wedge angle. This is to be compared to the approximate correction of 0.5° for the boundary-layer displacement effect applied in section 3.4.3.2. The predicted body points are also shown in Figure 3.20 as a terminator on each curve. The actual body position is indicated by a cross-hatched bar. It should be pointed out that the induction time phenomena which was observed previously (Hornung 1972a) is a small effect here. The flow field calculated by the method of characteristics (NMOCW), which is a direct method of calculating the flow, is also given in Figure 3.19. Here the vibrational energy is in equilibrium.

A fringe shift profile across the shock layer and normal to the shock, taken at 0.6cm from the tip of the wedge is shown in Figure 3.20. The profile is chosen to be close to the tip to minimise the distortion of the fringe due to three-dimensional effects. Here the fringe shift, calculated by the inverse method, according to all three sets of reaction rates is compared with experiment. It is immediately clear that the experimental results are quite unable to

resolve the difference in fringe shift predicted by the three rates. Contrast this with Figure 3.21 which compares the three shock curvature versus shock angle profiles, found by NMOCW according to the three sets of reaction rates, with experiment for both the 41.5° and 42.5° wedges. It is clear that the shock curvature measures the reaction rates more accurately, particularly at the tip, than the fringe shift, under the present conditions.

3.4.5 Summary

The influence of relaxation effects due to dissociation on hypersonic wedge flows of nitrogen is studied experimentally. The curved shock wave and relaxation zone characterized by a rise of density can be seen clearly in interferograms of the flow. The shock curvature at the tip of the wedge is a more sensitive indication of the dissociation rate than interferometric measurements of the density after the shock, under the conditions of the present experiments.

The results of Crane (1975) for the relative species concentrations of N_2 , N and He are used to calculate the free-stream for the wedge-flow experiments. It is found that the previous discrepancy between theoretical and experimental shock curvature at the highest enthalpy (Kewley 1971 and Kewley and Hornung 1974b) can be resolved by including helium contamination. Although no new dissociation rates are deduced from the experiments, it is seen that there is reasonable agreement with previous determinations; the highest temperature being 1460K.

3.5 Summary of Experimental Results

In this chapter, experimental studies of vibrational and chemical relaxation of nitrogen behind normal shocks, in

nozzle flows and over a wedge are made. The projects suggested by the Historical Review and listed in section 1.3 have been attempted, using the free-piston shock tube DDT and the free-piston shock tunnels T2 and T3. Optical interferometry is the main diagnostic tool for studying these flows.

The shock tube experiments in pure nitrogen confirm the strong temperature dependence of the pre-exponential factor of undiluted N_2 dissociation rates reported by Hanson and Baganoff (1972) over a temperature range of 6000-14000K. The reason for this effect could be due to V-V effects, which are at their greatest in undiluted diatomic gases.

The vibrational de-excitation rate of nitrogen is found to be equal to the shock-tube-determined value of Millikan and White (1963a), within a factor of ten, i.e. $\frac{1}{10} < \phi < 10$. The vibrational excitation rate of N_2 by N is found to be less than 50 times faster than the N_2 by N_2 rate, over a temperature range 7000-10300K. Both measurements are made in the small free-piston shock tunnel T2.

The dissociation rates of nitrogen flow over a wedge are investigated in the large free-piston shock tunnel using the shock curvature technique (also used in T2). The discrepancy, reported by Kewley and Hornung (1974b), between theory and experiment at the highest enthalpy is found to be resolved by including helium contamination in the free-stream. The results of Crane (1975) are used to calculate the contaminated flows. Agreement between theory and experiment, for accepted dissociation rates, of the shock curvature is reasonable.